Available online at www.sciencedirect.com

jmr&t Journal of Materials Research and Technology

journal homepage: www.elsevier.com/locate/jmrt

Original Article

Study of phase composition, photocatalytic activity, and photoluminescence of TiO_2 with Eu additive produced by the extraction-pyrolytic method

Vera Serga [a,b], *Regina Burve* [a,b], *Aija Krumina* [b], *Viktorija Pankratova* [a], *Anatoli I. Popov* [a], *Vladimir Pankratov* [a,*]

[a] *Institute of Solid State Physics, University of Latvia, Kengaraga 8, Riga, LV-1063, Latvia*

[b] *Institute of Inorganic Chemistry, Faculty of Materials Science and Applied Chemistry, Riga Technical University, P. Valdena 3/7, Riga, LV-1048, Latvia*

ARTICLE INFO

Article history:
Received 23 January 2021
Accepted 11 June 2021
Available online 17 June 2021

Keywords:
Extraction-pyrolytic method
Nanocrystalline TiO_2
Eu^{3+}
Degradation of methylene blue
Photoluminescence

ABSTRACT

Due to the unique properties and wide array of applications of nanocrystalline materials based on titanium dioxide, the study of new synthesis approaches remains relevant. In this study, within the framework of the extraction-pyrolytic method (EPM), we suggest using the mixtures of Ti- and Eu-containing organic extracts based on valeric acid as precursors for fabrication of nanocrystalline TiO_2-based powders with different Eu content: 0.5 mol%, 5 mol%, and 50 mol%. The thermal behavior of individual metal-containing extracts and their mixture was studied by thermogravimetric analysis and differential scanning calorimetry (TGA–DSC). To characterize phase composition and morphology of produced materials, the X-ray diffraction (XRD) method and scanning electron microscopy (SEM) were used. Photoluminescence properties of Eu^{3+} ions in TiO_2 nanocrystals have been studied. Photocatalytic activity of produced materials was tested in the reaction of methylene blue (MB) oxidation under UV-VIS irradiation. Correlation between synthesis parameters (Eu content and pyrolysis temperature) and properties of produced materials (phase composition, photoluminescence and photocatalytic properties) has been studied. It was demonstrated that the presence of a Eu-containing extract in the precursor mixture increases the anatase-to-rutile phase transformation temperature. The highest efficiency (degradation degree of MB 96%) was shown by TiO_2 powder consisting of mixed polymorphs, anatase (main phase) and rutile, with 0.5 mol% Eu additive. It was shown that anatase-to-rutile phase transformation in TiO_2:Eu^{3+} nanoparticles manifests in a degradation of Eu^{3+} luminescence intensity.

* Corresponding author.
E-mail address: Vladimirs.Pankratovs@cfi.lu.lv (V. Pankratov).

https://doi.org/10.1016/j.jmrt.2021.06.029

1. Introduction

Nanocrystalline titanium dioxide (TiO_2) has many applications due to its optical, thermal, photocatalytic, and electrophysical properties [1,2]. For instance, nanocrystalline TiO_2 is utilized in dye-sensitized solar cells, hydrogen production and storage, sensors, rechargeable batteries, self-cleaning and antibacterial surfaces. Currently, the most active research is related to the photocatalytic activity of TiO_2 nanoparticles for the environmental cleanup of organic pollutants. Due to chemical stability, non-toxicity, and low cost TiO_2 is considered the most promising photocatalyst for the degradation of pollutants in water and air [3–6].

TiO_2 has three naturally occurring polymorphs: rutile, anatase with the tetragonal crystal lattice, and brookite with the orthorhombic crystal lattice [7,8]. Rutile is more thermodynamically stable than anatase and brookite, which can be irreversibly transformed into the stable rutile phase by heat treatment in the temperature range from 400° to 1200 °C. Herewith, the temperature value is determined not only by the material synthesis technique but also by the method of determination of the transition temperature [7]. The stability of crystalline modifications also depends on the size of crystallites. According to the data reported in [9], anatase has higher thermodynamic stability if the particle size of TiO_2 does not exceed 35 nm.

TiO_2 belongs to the class of wide-band-gap semiconductors with band gap energy at 3.0–3.3 eV depending on the structure [10]. Thus, all of the above-mentioned polymorphs absorb light only in the ultraviolet (UV) spectral range with an absorption onset higher than 3 eV [11]. This fact limits the use of TiO_2 as a photocatalyst in the visible (VIS) region. The key parameter of photoactivity of TiO_2 is its phase composition [12]: anatase usually exhibits higher photocatalytic activity than rutile. Moreover, the crystallinity of TiO_2 in the anatase polymorph form improves if synthesis temperature is increased. This leads to the enhanced photocatalytic activity of the final product [13]. However, such heat treatment leads to the anatase-to-rutile phase transformation, which plays a negative role in photocatalytic activity. Hence, it is important to improve the thermal stability of the anatase phase in the synthesis process. There are two typical ways to achieve this purpose: the synthesis method modification or the addition of dopants [14,15]. Usually, transition, rare-earth metals (RE) and nonmetal ions (C, N, S, F) are used as dopant materials in TiO_2 [16]. The incorporation of the RE metal dopants including trivalent europium ion (Eu^{3+}) usually leads to the improvement of the photocatalytic behavior of TiO_2 in UV and VIS spectral range [17,18]. Moreover, Eu^{3+} doped TiO_2 is also considered a promising material for solar cells [19,20]. Besides, intensive red photoluminescence of Eu^{3+} in crystalline host matrices can be used to probe the local environment of the Eu^{3+} ion [21]. On the other hand, the influence of surface states on luminescence properties of the RE in nanoparticles has significant interest for fundamental research of nanophosphors [22–26]. Furthermore, a possible relationship between luminescent properties and photocatalytic efficiency of TiO_2 nanoparticles needs further investigations.

One of the popular methods for the synthesis of undoped and RE doped TiO_2 is the sol–gel method. This method allows production of homogeneous metal oxide nanoparticles [27] as well as facilitates the addition of dopants [18,28–31]. Titanium (IV) alkoxides or inorganic salts and RE inorganic salts are used as raw materials for RE-doped TiO_2 synthesis. However, the difference in the rates of hydrolysis of raw materials makes it difficult to control the synthesis, which can lead to the formation of material with segregated phases instead of the formation of the desired homogeneous structure of the polymer gel [32]. For RE-doped TiO_2 such solution techniques as co-precipitation [33,34] and hydrothermal [6,15,30,35] methods have been used.

The use of organic extracts based on saturated fatty acids as a new type of precursors is proposed in the framework of the extraction-pyrolytic method (EPM) to produce oxide materials for various functional purposes [36]. Synthesis of complex oxide materials by EPM includes the following main steps – extraction of metal ions from an aqueous solution with carboxylic acid (with or without a diluent), mixing the extracts in the required ratio, and subsequent pyrolysis. Herewith, EPM ensures the homogeneity of the materials produced, does not require the use of complex equipment and high costs for raw materials. The advantages of the method also include its versatility – production of nanocrystalline materials both as powders and films on various substrates and composites [36–41].

This work aim is producing TiO_2 with different Eu additives by EPM using mixtures of Ti- and Eu-containing extracts based on valeric acid. Besides, we are going to elucidate the effect of the ratio of the metals in the initial mixture of precursors and the temperature of its pyrolysis on the phase composition, photocatalytic, and luminescence properties of the final nanocrystalline powders.

2. Experimental

2.1. Sample preparation

To prepare individual solutions of metal valerates in valeric acid (extracts), the method of exchange extraction by fatty acids (HR) with the addition of alkali was used [42]. Trivalent metal ions extraction takes place according to the cation exchange mechanism and can generally be described by equation (1):

$$Me^{3+} + (3+s)HR + qH_2O \leftrightarrow [MeR_3 \cdot sHR] \cdot qH_2O + 3H^+, \quad (1)$$

where s and q – solvation and hydration numbers, respectively.

The extraction of metal ions was carried out from aqueous solutions of their salts, $Eu(NO_3)_3$ and $TiCl_3$, with a metal concentration of 1 M and 0.1 M, respectively. Valeric acid C_4H_9COOH without diluent was used as an extractant, and a solution of 1 M NaOH was used as an alkaline agent. The initial ratio of the aqueous (Aq) and organic (O) phases in the system was $Aq{:}O = 1{:}1$ and $Aq{:}O = 5{:}1$ for extraction of europium and titanium, respectively. Titanium chloride in hydrochloric acid solution (pH 0.5) was prepared right before extraction by

dissolving titanium powder in a HCI (1:1) solution followed by dilution with distilled water to a predetermined concentration. During the extraction process, with the gradual addition of NaOH solution, the organic phase slowly acquired a deep blue color. This indicates an increase in the concentration of Ti (III) valerate $Ti(C_4H_9COO)_3$ in the organic phase (Eq. (1)). Upon completion of the extraction, phase separation, and filtration of the obtained extract, its discoloration was observed. This is related to the oxidation of Ti (III) to Ti (IV) by atmospheric oxygen. It should be noted that in the presented work, no special studies to determine the final composition of the titanium (IV) carboxylate in organic solution were carried out. The pH of aqueous solutions measured after separation from the organic phase was ~1.2 for the extraction system with titanium and ~2.8 for the extraction system with europium. The obtained extracts were stable true solutions, and their storage did not require special conditions. The concentration of metals in organic solutions was determined by the gravimetric method [43] and was established to be 0.420 M for Ti-containing extract (E1) and 0.497 M for Eu-containing extract (E2).

Heat treatment (pyrolysis) of aliquots of extracts E1 and E2, as well as mixtures of E1 and E2 corresponding to 0.5 mol% of Eu (mixture M1), 5 mol% (mixture M2), and 50 mol% (mixture M3) in the final product, was carried out by heating in the air from room temperature to temperature (T_{pyr}) 550°-850 °C at a rate of 10°/min and annealed for 60 min. This was followed by powder rapid cooling at ambient conditions.

2.2. *Characterizations*

The thermal stability of the produced extracts and their mixture in static air was investigated by thermogravimetric analysis (TGA) and high temperature differential scanning calometry (HDSC) at a heating rate of 5 °/min (LINSEIS STA PT 1600). The phase composition of as-prepared samples was determined by the X-ray diffraction method (XRD) using a diffractometer D8 Advance (Bruker) with CuKα radiation ($\lambda = 1.5418$ Å). The XRD patterns were referenced to the PDF ICDD 00-034-0392 for europium oxide (Eu_2O_3), PDF ICDD 00-021-1272 for titanium dioxide (TiO_2) anatase phase, PDF ICDD 00-021-1276 for titanium dioxide (TiO_2) rutile phase, and PDF ICDD 01-070-7156 for europium titanate ($Eu_2Ti_2O_7$) identification. The mean crystallite size (d) of anatase (d_A), rutile (d_R), Eu_2O_3 (d_E) and $Eu_2Ti_2O_7$ (d_T) phases was calculated using the Scherrer method using most intense diffraction peaks corresponding to crystallographic planes (1 0 1), (1 1 0), (2 2 2), and (2 2 2), respectively. Weight fraction of the rutile phase (W_R) was determined by Gribb and Banfield [44] using integrated intensities A (areas) of most intense diffractions peaks as well (Eq. (2)).

$$W_R = A_R / (0.884A_A + A_R) \times 100\% \quad (2)$$

The surface morphology of the produced samples was studied by scanning electron microscopy (SEM) using the Helios 5 UX Thermo Scientific in SE mode with TLD detector.

Photocatalytic activity of produced powders was investigated by observing the degradation of methylene blue (MB) under UV-VIS irradiation. Experimental conditions and processing of the results were performed as described in [45]. 50 mg of produced material was added as a photocatalyst to 50 mL of 3.6 mg/L MB solution. For adsorption–desorption equilibrium, the suspension was stirred for 30 min in dark. Then it was photo-irradiated by UV-VIS light source (Osram Vitalux lamp, 300 W) for 30 min. The distance between the lamp source and the suspension was 11 cm. Degradation of methylene blue was observed by UV-VIS spectroscopy ($\lambda = 662$ nm) every 10 min. The whole test lasted 60 min. The kinetics of photocatalytic degradation of MB was expressed with pseudo-first-order constant of photocatalytic reaction k (s^{-1}):

$$k = \ln(C/C_0) / t, \quad (3)$$

where.

C is the concentration of MB after irradiation;
C_0 – the initial concentration of MB solution;
t – the irradiation time.

Luminescence spectra, as well as luminescence excitation spectra, of produced samples have been measured using Photoluminescence Spectrometer FLS1000 (Edinburgh

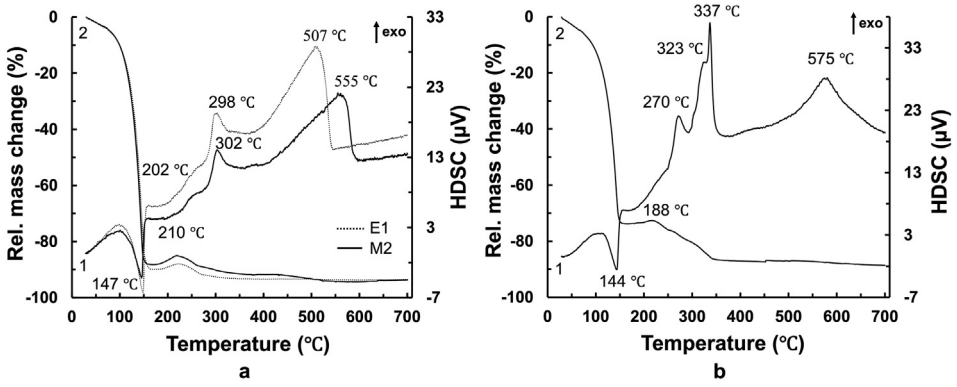

Fig. 1 – Thermal behaviour of Ti-containing extract E1 and its mixture M2 with Eu-containing extract (a), Eu-containing exstract E2 (b): 1 – HDSC; 2 – TG.

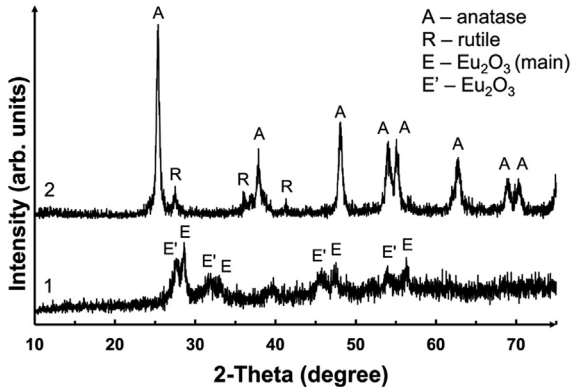

Fig. 2 – XRD patterns of thermal decomposition products of extracts: 1 – Eu-containing extract (E2); 2 – Ti-containig extract (E1). T_{pyr} = 550 °C.

Instruments). The experiments have been carried out at room temperature.

3. Results and discussion

3.1. *Thermal stability of extracts*

Ketones and the corresponding metal oxides are the main products of the thermal decomposition of salts of many carboxylic acids as established earlier in Ref. [46]. The thermal stability of metal carboxylates and the mechanism of their decomposition depend on the length of the carboxylic acid hydrocarbon radical and the nature of the metal [47]. Therefore, to determine the minimal pyrolysis temperature of a mixture of extracts for producing oxide powders of various compositions, we studied the thermal behavior of both individual extracts (Fig. 1a, E1 and Fig. 1b) and their mixture corresponding to the Eu content in the final product of 5 mol% (Fig. 1a, M2).

At the beginning of the heating process, all studied samples are characterized by the same thermal behavior: the first weight loss occurs starting from ~30 °C and is associated with the evaporation of free extractant (solvent). In the region of the first endothermic peaks in the temperature ranges of ~105°–160 °C (Fig. 1a) and ~120°-149 °C (Fig. 1b), evaporation processes of both solvent and co-extracted water take place. Thereafter, the thermal transformations of samples E1 (Fig. 1a, E1) and E2 (Fig. 1b) are determined by the thermal behavior of the metal carboxylates and differ significantly.

Thermal destruction of Ti-containing extract E1 (Fig. 1a, E1) starts at a temperature of ~147 °C (the maximum of the first endothermic peak), and weight loss of the sample is observed up to 160 °C. Upon further heating, the wide asymmetric endothermic peak at 202 °C is observed on the HDSC curve, while the TG curve first maintains a constant sample mass, and then its slight increase (~1.7%). Such thermal behavior of the sample is probably associated with thermal transformations of the resulting decomposition intermediates: the endothermic evaporation process of gaseous products (most likely, carbon dioxide CO_2) and the exothermic process of the gradual oxidation of TiO to TiO_2 [41,48]. The weight loss (~4.2%) observed in the temperature range ~225°–280 °C is associated with the thermal decomposition of an organic matter. In the area of the exothermic peak (~280°–320°C), combustion of the residue of gaseous products occurs, which is accompanied by an insignificant weight loss (0.7%). With an increase in temperature above 350°C, the mass of the sample practically does not change. An exothermic peak observed in the temperature range ~400°–540 °C is associated with the beginning of crystallization of titanium dioxide and its subsequent polymorphic transformations.

After evaporation of the solvent and co-extracted water during further heating of extract E2 (Fig. 1b), the sample mass remains almost constant in the temperature range ~149°–217 °C. An elongated endothermic peak (~159°-203 °C) is observed on the HDSC curve can be associated with the melting of the europium (III) valerate $Eu(C_4H_9COO)_3$ [49]. Starting from 217 °C and up to 344 °C, an active (about 14%) weight loss of the sample is observed, which is directly related to the thermal destruction of the metal valerate. It was found [49,50] that thermal transformations of individual carboxylates of rare earth elements (RE) into the corresponding sesquioxides proceed via an intermediate stage of the formation of metal dioxymonocarbonate and the release of ketone and CO_2. When the temperature reaches 550 °C, the mass of the sample is practically constant. In the temperature range ~553°–608 °C, an intense broad exopeak is observed on the HDSC curve, which is associated with the crystallization of the final product and the burnout of carbon formed as a result of the combustion of gaseous decomposition products.

The presence of the Eu-containing extract E2 in the mixture M2 (Fig. 1a, M2) leads to the changes in the thermal behavior of the extract E1 – the weight loss of the sample ends at a higher temperature of ~520 °C, and the exothermic peaks on the HDSC curve shift from 298° to 302 °C (the first exopeak) and from 507° to 555 °C (second exopeak).

Thus, the thermal behaviour of Ti-containing (E1) and Eu-containing (E2) extracts is characterized by different mechanisms, which, in turn, affects the thermal stability of the

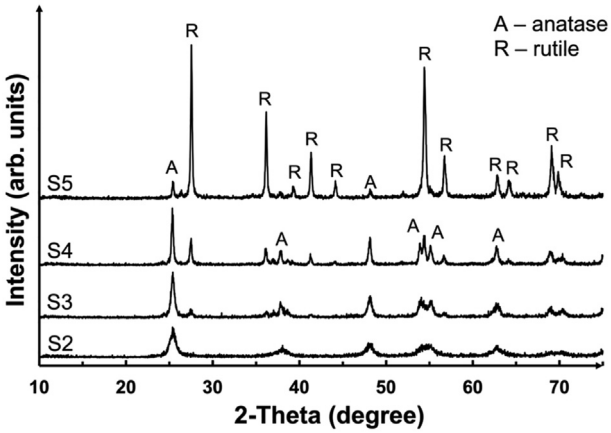

Fig. 3 – XRD patterns of pyrolysis products of extract mixture M1 (corresponding to 0.5 mol% Eu additive to TiO_2) produced at different T_{pyr}: S2 – 550 °C; S3 – 650 °C; S4 – 750 °C; S5 – 850 °C.

Table 1 – Impact of synthesis conditions on phase composition and mean crystallite size of produced materials.

Sample Nr.	Synthesis conditions		Phase composition	d, nm	W, %
	Precursor	T_{pyr}, °C			
S1	E1	550	TiO_2 anatase	21	94
			TiO_2 rutile	~30	6
S2	M1	550	TiO_2 anatase	11	100
S3		650	TiO_2 anatase	20	90
			TiO_2 rutile	~30	10
S4		750	TiO_2 anatase	35	64
			TiO_2 rutile	36	36
S5		850	TiO_2 anatase	~40	8
			TiO_2 rutile	45	92
S6	M2	750	TiO_2 anatase	12	96
			TiO_2 rutile	~20	4
S7		850	TiO_2 anatase	Discerned	–
			TiO_2 rutile	40	
			$Eu_2Ti_2O_7$	36	
S8	M3	750	Amorphous	–	–
S9		800	$Eu_2Ti_2O_7$	38	–
S10		850	$Eu_2Ti_2O_7$	40	–

mixture of extracts M2 (Fig. 1a, M2). Based on the results obtained, a temperature of 550 °C was established to be a minimal pyrolysis temperature in this study.

3.2. *Characterization of produced materials*

3.2.1. *Phase composition*

XRD analysis of the pyrolysis products of individual extracts E1 and E2 is shown in Fig. 2. The thermal treatment at 550 °C of extract E1 leads to the formation of nanocrystalline TiO_2 powder, consisting of anatase and rutile polymorphs (Table 1, sample S1), but of extract E2 – europium oxide Eu_2O_3 also containing two crystalline phases.

The main phase (E) of Eu_2O_3, identified by PDF ICDD 00-034-0392, has a crystal lattice parameter a = 10.868 Å. The diffraction peak maxima of the second phase (E') are noticeably shifted to the region of lower values of 2-Theta angles (a = 11.250 Å). According to an approximate estimate, the average crystallite size of both main and additional phases is 15 nm and 10 nm, respectively. It should be noted that with an increase in the pyrolysis temperature from 550 °C to 750 °C of the Eu-containing extract, a gradual increase in the content of the main phase of Eu_2O_3 is observed, and after treatment at 750°C, the second additional phase was not detected in the X-ray diffraction pattern. In this case, d_E of the main phase increases to 30 nm. Thus, the results of the X-ray phase analysis presented in Fig. 2 do not contradict the results of TG-HDSC analysis (Fig. 1a, E1 and Fig. 1b).

The results of XRD analysis of samples produced by pyrolysis of mixtures of extracts E1 and E2 are summarized in Table 1.

Analysis of the data obtained shows that an increase in the content of the Eu-containing extract E2 in the mixture not only slows down the anatase-to-rutile phase transformation (samples S4 and S6) but also leads to a change in the phase composition of the final pyrolysis products (samples S7 and S10).

It was found (Fig. 3) that at a low content of extract E2 (mixture M1), an increase in the pyrolysis temperature facilitates the anatase-to-rutile phase transformation (Table 1) and leads to an increase in d of both crystalline phases of TiO_2. However, even at a temperature of 850 °C, a complete transformation is not observed (anatase weight fraction ~8%). The thermal treatment of the mixture M1 at a minimal temperature of 550 °C, in contrast to the pure extract E1, makes it possible to fabricate monophase TiO_2 with the anatase crystal structure.

With an increase in the Eu content to 5 mol% (mixture M2), beginning temperature of anatase-to-rutile phase transformation shifts even more significantly to 750 °C (Fig. 4, sample S6; Table 1). Moreover, an increase in temperature by 100 °C leads to almost complete phase transformation and simultaneous crystallization of an additional phase – europium titanate $Eu_2Ti_2O_7$ (Fig. 4, sample S7; Table 1).

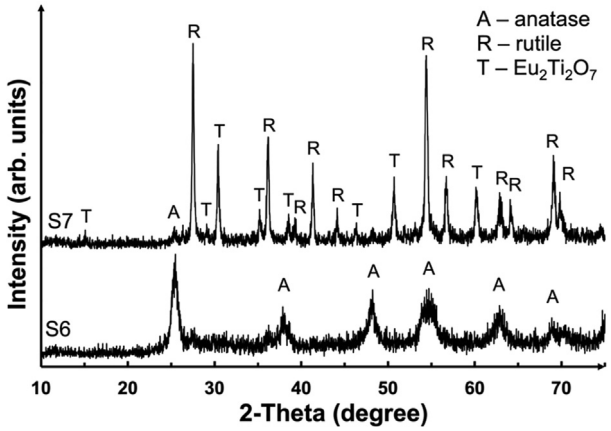

Fig. 4 – XRD patterns of pyrolysis products of extract mixture M2 (corresponding to 5 mol% Eu additive to TiO_2) produced at different T_{pyr}: S6 – 750 °C; S7 – 850 °C.

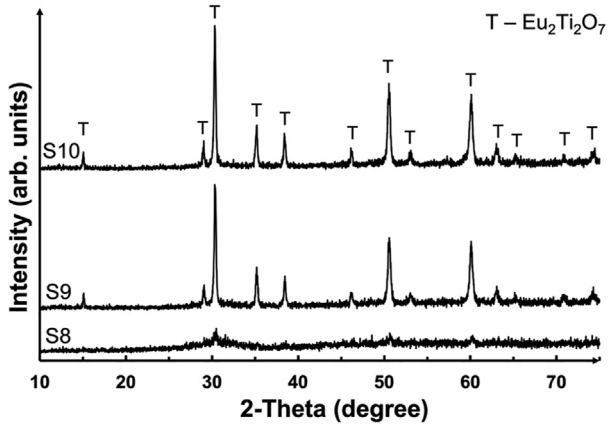

Fig. 5 – XRD patterns of $Eu_2Ti_2O_7$ samples produced from equimolar mixture of extracts M3 at different T_{pyr}: S8 – 750 °C; S9 – 800 °C; S10 – 850 °C.

Thus, based on the presented results of TGA-HDSC (Fig. 1) and XRD (Figs. 3 and 4; Table 1) analyses, it is evident that the presence of the thermally more stable extract E2 in the initial mixture of extracts in comparison with extract E1, inhibits the crystallization and growth of anatase particles, that consequently increases the temperature of the anatase-to-rutile phase transformation. Moreover, the higher is the Eu content in the extract mixture, the higher is the temperature of the beginning of this transition. Similar regularities on the effect of the RE additive on the phase transformation were also reported in the studies [14–18].

Due to the large difference in ionic radii (Ti^{4+} – 0.64 Å and Eu^{3+} – 0.95 Å) europium ions can be incorporated into the TiO_2 lattice interstitially or can form a thin oxide layer on the surface of the TiO_2 particles [14]. Anatase-to-rutile transformation involves cleavage and rearrangement of the Ti–O bonds, thus, if Eu ions incorporate interstitially, the ionic mobility is hindered, which prevents the phase transformation. On the other hand, the presence of Eu_2O_3 on the surface of the TiO_2 particles inhibits the growth of the anatase particles. This creates difficulties for its agglomeration and prevents achieving the anatase particles' critical size (14 nm [9]) for rutile formation. We assume that using EPM, the influence of Eu additive on the anatase-to-rutile phase transformation involves both described mechanisms.

Thermal treatment of an equimolar mixture of extract M3 allows producing crystalline $Eu_2Ti_2O_7$ starting from a temperature of 800 °C (Fig. 5; Table 1 samples S8 and S9). Moreover, an increase in temperature to 850 °C practically does not affect the value of d_T. Thus, based on the results obtained, we can assume the presence of europium titanate in

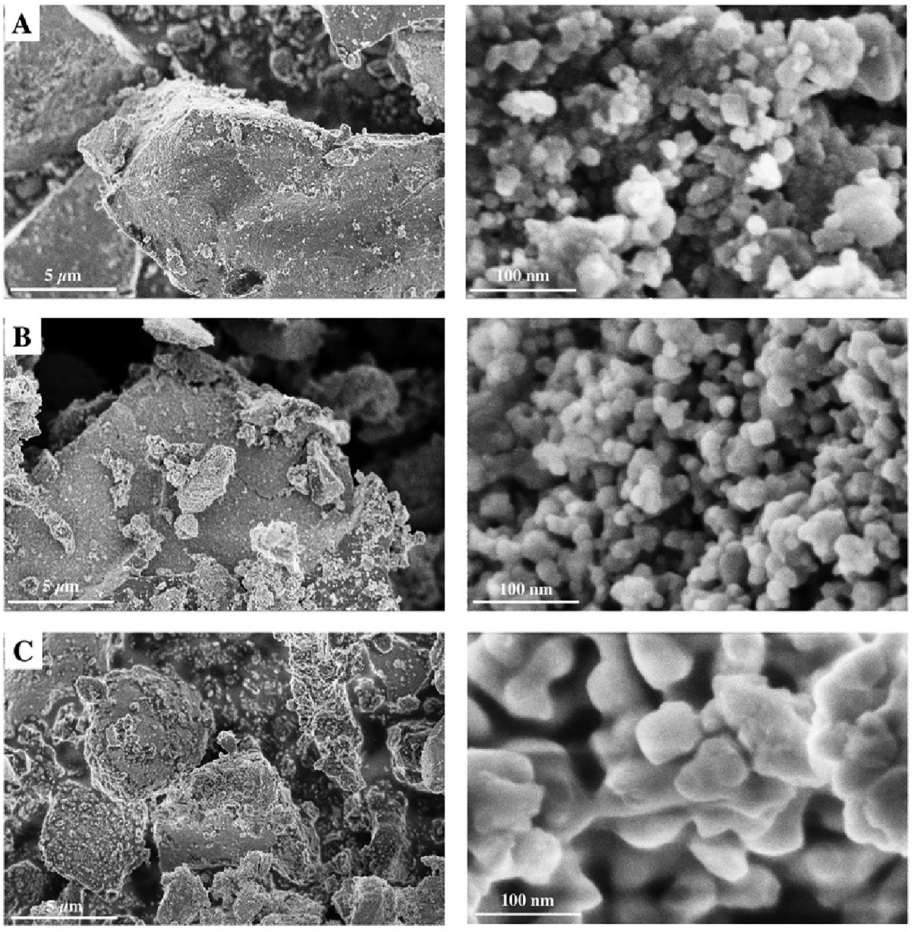

Fig. 6 – SEM images of the produced samples: A – pure TiO_2 (S1), B–TiO_2 with 0.5 mol% Eu additive (S3), C–TiO_2 with 5 mol% Eu additive (S6). Magnification for images in a left column – ×10 000, in a right column – ×500 000.

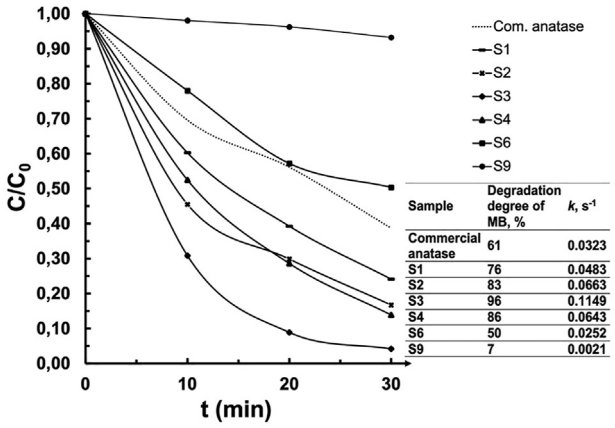

Sample	Degradation degree of MB, %	k, s^{-1}
Commercial anatase	61	0.0323
S1	76	0.0483
S2	83	0.0663
S3	96	0.1149
S4	86	0.0643
S6	50	0.0252
S9	7	0.0021

Fig. 7 – The degradation degree of MB and rate constant of produced samples in comparison with commercial anatase.

sample S5 (Table 1, Fig. 3), which due to its low content is not detected by XRD.

3.2.2. *Morphology*

The shape and surface morphology of the synthesized nanocrystalline TiO_2 powders were studied using SEM, and the results are represented in Fig. 6. Investigations were performed for the samples of pure TiO_2 and TiO_2 with 0.5 and 5 mol% Eu additive, phase composition (anatase-rutile ratio) of which is similar (samples S1, S3 and S6, see Table 1). The synthesized TiO_2 powders consist of irregular rock-like agglomerates having a large variations in size and shape (Fig. 6, left column). Presented images show that Eu additives in TiO_2 samples S3 and S6 lead to the formation of more loose agglomerates despite a higher T_{pyr} than in the case of the pure TiO_2 (sample S1). The high magnification image (Fig. 6, A, right column) of pure TiO_2 powder (sample S1) showed that agglomerates consist of round-shaped and some faceted particles with approximate size from 7 to 25 nm. An increase in T_{pyr} by 100 °C and the presence of 0.5 mol% Eu additive (sample S3) did not lead to a significant change in the morphology and size of the TiO_2 particles (Fig. 6, B, right column). However, in agglomerates a well-defined interface between predominantly spherical particles can be traced. As a result of a further increase in the processing temperature and the europium content (sample S6), the formation of densely packed agglomerates possessing branched structure is observed. Based on the results of XRD analysis (see Fig. 4, sample S6), this powder is poorly crystallized. Therefore, it can be assumed that these structures are formed from amorphous phases (TiO_2 and $Eu_2Ti_2O_7$) containing nanocrystalline TiO_2 particles as inclusions.

3.2.3. *Photocatalytic activity*

The study results of the influence of the synthesis conditions (Table 1) on photocatalytic activity of produced samples are shown in Fig. 7. For comparison, the results for commercial TiO_2 powder with anatase structure and $d_A < 25$ nm (Sigma–Aldrich) are also presented.

The degradation degree of MB of pure TiO_2 sample S1 ($W_A = 96\%$) produced at 550 °C is 76% ($k = 0.0483\ s^{-1}$). Sample S2 with the crystal structure of anatase containing 0.5 mol% of Eu additive (Table 1) leads to an increase in both degradation degree and rate constant to 83% and to 0.0663 s^{-1}, respectively. This sample has better activity than commercial anatase, and its rate constant is almost two times greater.

In series of TiO_2 samples with 0.5 mol% Eu additive (samples S2–S4) an increase in production temperature from 550 °C to 750 °C leads to a change in photocatalytic activity, which is not monotonic. Wherein, these samples are characterized by better photocatalytic activity than pure TiO_2 (sample S1) or commercial anatase. In the case of sample produced at 650 °C (sample S3), the best photocatalytic activity is achieved, and degradation degree of MB is 96% ($k = 0.1149$). It should be mentioned that, excluding the presence of Eu, sample S3 is quite similar to S1 in both phases ratio and its mean crystalline size (Table 1). Thus, the improvement in photocatalytic activity is probably associated with the presence of europium additive.

Improving TiO_2 photocatalytic activity by doping with RE ions, including Eu ions, was also reported in [15,18,31,51]. This evidence can be related to the synergetic effect of improved absorption and charge separation (due to 4f electron configurations of RE elements) as well as to an enhanced

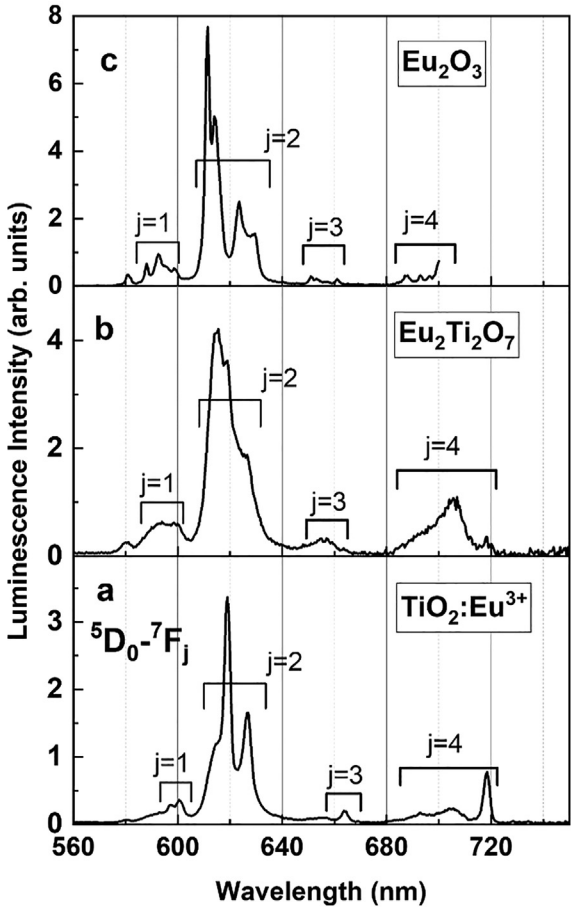

Fig. 8 – Luminescence spectra of TiO_2:Eu^{3+} nanoparticles (sample S2) (a), $Eu_2Ti_2O_7$ nanoparticles (sample S9) (b) and Eu_2O_3 nanoparticles (c) under excitation of $^7F_0$ - $^5D_2$ transition in Eu^{3+}.

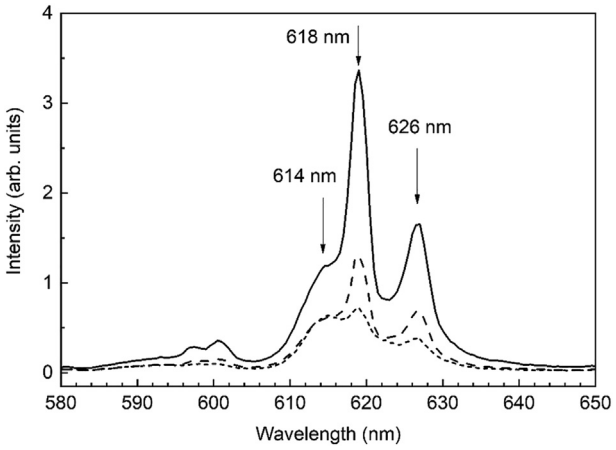

Fig. 9 – The comparison of emission lines due to $^5D_0$ - $^7F_2$ transitions under excitation of $^7F_0$ - $^5D_2$ in $Eu^{3+}$for the samples S2 (solid line), S3 (dashed line) and S4 (short dashed line).

photocatalytic activity of TiO_2 under VIS irradiation due to red shifts of the optical absorption edge.

For samples produced at 750 °C (S4 and S6) increase in europium content from 0.5 to 5 mol% leads to an increase in anatase weight fraction (Table 1), but in a decrease in both degradation degree and rate constant. In this case, photocatalytic activity of sample S6 was worse also in comparison with pure TiO_2 (sample S1) and commercial anatase. It can be explained by the contrasting morphology (see Fig. 6, C) and the presence of amorphous $Eu_2Ti_2O_7$, which is a photocatalytically inactive material (Fig. 7, S9).

3.2.4. *Luminescence properties*

Figure 8 (a) exhibits emission spectra of europium doped TiO_2 (Table 1, sample S2) nanoparticles while the emission spectra of $Eu_2Ti_2O_7$ (Table 1, sample S9) and Eu_2O_3 (Fig. 2, curve 1) nanoparticles are shown in Fig. 8 (b, c), respectively, for comparison. The emission lines due to the $^5D_0$ - ^7F_J transition are observed in all samples studied under excitations of $^7F_0$ - $^5D_2$ transitions (466 nm excitation). The Eu^{3+}-doped TiO_2 nanocrystals exhibit emissions clearly different from those observed in Eu_2O_3 and $Eu_2Ti_2O_7$, in terms of line shapes and line positions, meaning different local environments of Eu^{3+} ions. It is known that both anatase (space group D_{4h}^{19}) and rutile (D_{4h}^{14}) assume tetragonal symmetry [8] while Eu_2O_3 (T_h^7) [52] and $Eu_2Ti_2O_7$ ($Fd\bar{3}m$) [53] have cubic symmetry at room temperature. In addition, the substitutional Eu^{3+} dopants in TiO_2 are less well-located on the lattice sites as compared to the Eu^{3+} ions in the latter two compounds (where Eu^{3+} is a part of main lattice), due to lattice distortion and the existence of point defects for instance oxygen vacancies. Thus, Fig. 8 provides clear evidence that the emissions from TiO_2:Eu^{3+} nanoparticles originates from the Eu^{3+} ions embedded into the TiO_2 lattice but not due to luminescence of Eu_2O_3 or $Eu_2Ti_2O_7$ samples.

Figure 9 shows the detailed comparison of the emission spectra ($^5D_0$ - $^7F_2$ transitions) of Eu^{3+} in TiO_2 nanoparticles having different content of anatase and rutile phases. The emission intensities as well as the shape of the emission spectra in Fig. 9 are dependent on the pyrolysis temperature. The intensity of Eu^{3+} emission lines decreases if pyrolysis temperature increasing. It means that the emission intensity is lower in those TiO_2 nanocrystalline samples, which contain more rutile phase. The degradation of luminescence intensity passing from anatase to rutile phases of TiO_2 was reported before in [54,55]. The sharp luminescence lines peaking at 618 and 626 nm can be observed in all spectra depicted in Fig. 9. In addition, at least one extra line at 614 nm can be also resolved. However, a relative intensity of the 614 nm line is higher in the samples comprising more rutile phase in the lattice. This fact indicates that the disorder of the symmetry around the Eu^{3+} ions in the TiO_2:Eu^{3+} particles changes passing from the anatase to rutile phase.

Another possible explanation of the results depicted in Fig. 9 is related to the multisite Eu^{3+} centers. Indeed, the multisite luminescence of rare-earth ions in TiO_2 has been reported in literature [28,56,57]. Namely, three types of Eu^{3+} centers in TiO_2 were detected at low temperature (10 K). However, we were able to perform our experiments at room temperature only masking a possible multisite emission centers. In addition, it is worth noting that each type of the Eu^{3+} centers can be revealed in both the emission spectra and the excitation spectra. This means that, under certain excitations, the emission spectra can exhibit specific features of one of the three types of Eu^{3+} centers. For instance, three different Eu^{3+} centers have been shown in the emission spectra under slightly different excitations within $^5D_2$ (464.9 nm, 477.6 nm and 484.6 nm) as it was shown in [28]. On the other hand, the emission spectra depicted in Fig. 9 were measured under the same excitation wavelength, i.e. presumably exciting one type of the Eu^{3+}. Thus, the differences in the emission spectra in Fig. 9 are caused by the changing of the crystal structure rather than the multisite luminescence centers. However, we cannot exclude that the multisite Eu^{3+} centers are incorporated into the lattice of our TiO_2

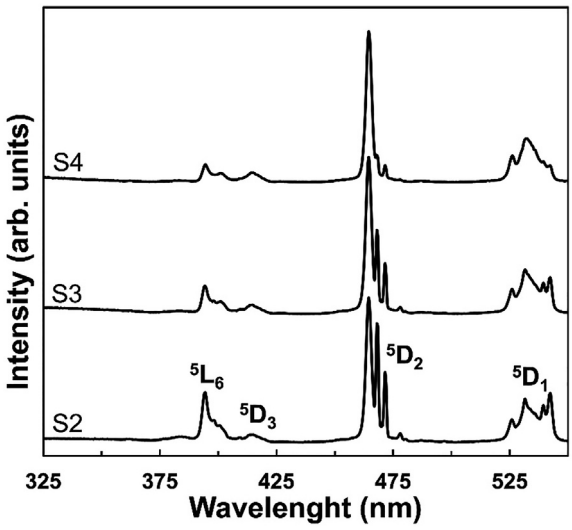

Fig. 10 – The excitation spectra for three samples of TiO^2:Eu^{3+} nanoparticles monitored at 618 nm. The spectra are normalized to the maximum intensity of the 466 nm line.

nanoparticles. These multisite Eu^{3+} centers cause to the distinguished structure of $^5D_2$ and $^5D_3$ bands observed in the excitation spectra below.

Figure 10 displays the excitation spectra of three Eu^{3+}-doped TiO_2 nanocrystalline samples measured by monitoring the 618 nm emission from the $^5D_0$ - $^7F_2$ transition of Eu^{3+} ions. The three groups of lines at 390–400, 460–470, and 530–550 nm, can be assigned to the $^7F_0$ - $^5D_3$, $^7F_0$ - $^5D_2$, $^7F_0$ - $^5D_1$ and $^7F_0 - {}^5L_6$ transitions of the Eu^{3+} ions, respectively [58]. The most noticeable differences among excitation spectra are observed for $^5D_2$ and $^5D_3$ bands. The main line of $^5D_2$ for all three sample (Fig. 10) is located at the same spectral position. However, for each excitation spectrum the main $^5D_2$ is accompanied by two extra lines at lower energy side. The relative intensity of these extra lines in respect of the main $^5D_2$ is sample dependent, i.e. they decrease with increasing particle diameter. We can speculate that multisite Eu^{3+} centers are responsible for the triplet structure of $^5D_2$ band in the excitation spectra indicating three types of Eu^{3+} centers by analogy with known literature data [28,56,57]. We suppose that two types of Eu^{3+} centers are located close to the surface of nanoparticles and, therefore, they disappear with increasing particle size. In principle the same analysis can be also addressed to the $^5D_3$ bands. In order to confirm our suggestions low temperature experiments are foreseen in the near future.

It is worth noting that there are no excitation bands at energies higher than the $^7F_0 - {}^5L_6$ transitions. It means that there is no excitation band corresponding to the absorption band of pure TiO_2. This fact indicates that Eu^{3+} ions cannot be effectively excited through the TiO_2 host lattice but only after the absorption by the Eu^{3+} ions themselves. It is well accepted that the energy transfer from the TiO_2 host to Eu^{3+} ions is a defect-mediated process [59,60]. According to this model UV light is absorbed in the band gap of TiO_2 then electrons from conduction bands and holes valence are trapped by the defect states with subsequent energy transfer to Eu^{3+} states. We suggest that the concentration of surface defects in the TiO_2:Eu^{3+} nanoparticles obtained in current work is high and they act as a non-radiative relaxation centers suppressing Eu^{3+} emission. On the other hand, we suggest that these defects are responsible for high photocatalitic activity of TiO_2:-Eu^{3+} nanoparticles shown in Fig. 7.

4. Conclusions

The TGA-HDSC results showed that using a mixture of Ti- and Eu-containing extracts based on valeric acid as a precursor, the minimal pyrolysis temperature is determined by the more thermally stable Eu-containing extract. According to XRD analysis data, the presence of Eu-containing extract in a mixture of extracts inhibits anatase-to-rutile phase transformation: upon production temperature of phase transformation shifts from 550 °C for pure TiO_2 to 650 °C and 750 °C for TiO_2 with 0.5 mol% and 5 mol% of Eu additive, respectively. As a result of pyrolysis of an equimolar mixture of extracts at a temperature of 850 °C forms crystalline monophase europium titanate $Eu_2Ti_2O_7$ with $d_T = 40$ nm. At this pyrolysis temperature, the presence of the crystalline phase of $Eu_2Ti_2O_7$ as an impurity to the main rutile phase was also found in the pyrolysis products of a mixture of extracts corresponding to 5 mol% of Eu additive. During degradation of methylene blue under UV-VIS irradiation, sample produced at 650 °C with 0.5 mol% of Eu additive showed the highest photocatalytic activity with 96% degradation degree of MB ($k = 0.1149$). Luminescence experiments demonstrate that the photoluminescence properties of Eu^{3+} ion doped TiO_2 nanocrystals are phase sensitive. The degradation of luminescence intensity, as well as the altering of spectral shape of Eu^{3+} emission, was observed when anatase-to-rutile phase transformation of TiO_2:Eu^{3+} nanoparticles occurs. The Eu^{3+} luminescence can be exited under direct excitation of Eu^{3+} transitions, but it is not effective under UV excitations due to surface loss centers (defects). On the other hand, it is assumed that these defect centers can be responsible for the high photocatalytic activity of the TiO_2:Eu^{3+} nanoparticles.

Declaration of Competing Interest

The authors declare that they have no known competing financial interests or personal relationships that could have appeared to influence the work reported in this paper.

Acknowledgements

The Institute of Solid State Physics, University of Latvia as the Center of Excellence has received funding from the H2020-WIDESPREAD-01-2016-2017-TeamingPhase2 under grant agreement No. 739508, project CAMART2. The work was also partially supported by the LZP grant 2020/2-0074. R. Burve has been supported by the project "Synthesis of nanostructured materials based on titanium dioxide and tin dioxide and investigation of their physicochemical properties" Nr. MP-2019/7, for strengthening scientific personnel capacity 2019/2020 at the Riga Technical University. Authors are grateful to Dr. K. Šmits for the microscopic measurements and SEM images.

REFERENCES

[1] Khataee A, Mansoori GA. Nanostructured titanium dioxide materials: properties, preparation and applications. Hackensack: World Scientific Publishing; 2011.
[2] Gupta SM, Tripathi M. A review of TiO_2 nanoparticles. Chin Sci Bull 2011;56(16):1639–57.
[3] Martyanov IN, Klabunde KJ. Photocatalytic purification of water and air over nanoparticulate TiO_2. In: Klabunde KJ, Richards RM, editors. Nanoscale materials in chemistry. 2nd. ed. Hoboken: John Wiley & Sons; 2009. p. 581–604.
[4] Lin L, Chai Y, Zhao B, Wei W, He D, He B, et al. Photocatalytic oxidation for degradation of VOCs. Open J Inorg Chem 2013;3:14–25.
[5] Kumar S, Ahlawat W, Bhanjana G, Heydarifard S, Nazhad MM, Dilbaghi N. Nanotechnology-based water

treatment strategies. J Nanosci Nanotechnol 2014;14:1838–58.
[6] Ye J, Chao C, Hong J. Preparation of a novel nano-TiO_2 photocatalytic composite using insoluble wood flour as bio-carrier and dissolved components as accelerant. J Mater Res Technol 2020;9(5):11255–62.
[7] Hanaor DAH, Sorell CC. Review of the anatase to rutile phase transformation. J Mater Sci 2011;46:855–74.
[8] Evarestov RA, Smirnov VP. Supercell model of V-doped TiO_2: unrestricted Hartree-Fock calculations. Phys Status Solidi B 1999;215(2):949–56.
[9] Hengzholg Z, Banfield JF. Thermodynamic analysis of phase stability of nanocrystalline titania. J Mater Chem 1998;8(9):2073–6.
[10] Landmann M, Rauls E, Schmidt WG. The electronic structure and optical response of rutile, anatase and brookite TiO_2. Phys B Condens Matter 2012;24(19):195503.
[11] Katoh R, Murai M, Furube A. Transient absorption spectra of nanocrystalline TiO_2 films at high excitation density. Chem Phys Lett 2010;500:309–12.
[12] Ahmed AY, Kandiel TA, Oekermann T. Photocatalytic activities of different well-defined crystal TiO_2 surfaces: anatase versus rutile. J Phys Chem Lett 2011;2:2461–5.
[13] Bellardita M, Di Paola A, Megna B, Palmisano L. Determination of the crystallinity of TiO_2 photocatalysts. J Photochem Photobiol, A 2018;367:312–20.
[14] Setiawati E, Kawano K. Stabilization of anatase phase in the rare earth; Eu and Sm ion doped nanoparticle TiO_2. J Alloys Compd 2008;451(1–2):293–6.
[15] Rozman N, Tobaldi D, Cvelbar U, Puliyalil H, Labrincha J, Legat A, et al. Hydrothermal synthesis of rare-earth modified titania: influence on phase composition, optical properties, and photocatalytic activity. Materials 2019;12(5):713–32.
[16] Shayegan Z, Lee C-S, Haghighat F. TiO_2 photocatalyst for removal of volatile organic compounds in gas phase – a review. Chem Eng J 2018;334:2408–39.
[17] Liu H, Yu L, Chen W, Li Y. The progress of TiO_2 nanocrystals doped with rare earth ions. J Nanomater 2012;2012:235879.
[18] Khade GV, Gavade NL, Suwarnkar MB, Dhanavade MJ, Sonawane KD, Garadkar KM. Enhanced photocatalytic activity of europium doped TiO_2 under sunlight for the degradation of methyl orange. J Mater Sci Mater Electron 2017;28(15):11002–10.
[19] Farheen FH, Ansari SG, Khan AA, Ansari ZA. Europium doped TiO_2: an efficient photoanode material for dye sensitized solar cell. J Mater Sci: Mater El 2017;28(9):6873–9.
[20] Kumar V, Swami SK, Kumar A, Ntwaeaborwa OM, Dutta V, Swart HC. Eu^{3+} doped down shifting TiO_2 layer for efficient dye-sensitized solar cells. J Colloid Interface Sci 2016;484:24–32.
[21] Binnemans K. Interpretation of europium (III) spectra. Coord Chem Rev 2015;295:1–45.
[22] Pankratov V, Popov AI, Shirmane L, Kotlov A, Feldmann C. $LaPO_4$:Ce,Tb and YVO_4:Eu nanophosphors: luminescence studies in the vacuum ultraviolet spectral range. J Appl Phys 2011;110(5):053522.
[23] Shirmane L, Feldmann C, Pankratov V. Comparing the luminescence processes of YVO_4:Eu and core-shell YVO_4@YF_3 nanocrystals with bulk-YVO_4:Eu. Phys B Condens Matter 2017;504:80–5.
[24] Kuzmanoski A, Pankratov V, Feldmann C. Energy transfer of the quantum-cutter couple Pr^{3+}–Mn^{2+} in CaF_2:Pr^{3+}, Mn^{2+} nanoparticles. J Lumin 2016;179:555–61.
[25] Shirmane L, Pankratov V. Emerging blue-UV luminescence in cerium doped YAG nanocrystals. Phys Status Solidi RRL 2016;10(6):475–9.
[26] Kuzmanoski A, Pankratov V, Feldmann C. Microwave-assisted ionic-liquid-based synthesis of highly crystalline $CaMoO_4$:RE^{3+} (RE = Tb, Sm, Eu) and $Y_2Mo_4O_{15}$:Eu^{3+} nanoparticles. Solid State Sci 2015;41:56–62.
[27] Macwan DP, Dave PN, Chaturvedi S. A review on nano-TiO_2 sol-gel type synthesis and its applications. J Mater Sci 2011;46:3669–86.
[28] Antić Ž, Krsmanović RM, Nikolić MG, Marinović-Cincović M, Mitrić M, Polizzi S, et al. Multisite luminescence of rare earth doped TiO_2 anatase nanoparticles. Mater Chem Phys 2012;135(2–3):1064–9.
[29] Asal S, Saif M, Hafez H, Mozia S, Heciak A, Moszyński D, et al. Photocatalytic generation of useful hydrocarbons and hydrogen from acetic acid in the presence of lanthanide modified TiO_2. J Hydrog Energy 2011;36(11):6529–36.
[30] Đorđević V, Milićević B, Dramićanin MD. Rare earth-doped anatase TiO_2 nanoparticles. In: Janus M, editor. Titanium dioxide. IntechOpen; 2017. p. 25–60.
[31] Liang CH, Li FB, Liu CS, Lü JL, Wang XG. The enhancement of adsorption and photocatalytic activity of rare earth ions doped TiO_2 for the degradation of Orange I. Dyes Pigments 2008;76(2):477–84.
[32] Cividanes LS, Campos TMB, Rodrigues LA, Brunelli DD, Thim GP. Review of mullite synthesis routes by sol–gel method. J Sol Gel Sci Technol 2010;55(1):111–25.
[33] Zikriya M, Nadaf YF, Bharathy PV, Renuka CG. Luminescent characterization of rare earth Dy^{3+} ion doped TiO_2 prepared by simple chemical Co-precipitation method. J Rare Earths 2018;37(1):24–31.
[34] Xie Y, Yuan C. Characterization and photocatalysis of Eu^{3+}–TiO_2 sol in the hydrosol reaction system. Mater Res Bull 2004;39(4–5):533–43.
[35] Falcomer D, Daldosso M, Cannas C, Musinu A, Lasio B, Enzo S, et al. A one-step solvothermal route for the synthesis of nanocrystalline anatase TiO_2 doped with lanthanide ions. J Solid State Chem 2006;179(8):2452–7.
[36] Khol'kin AI, Patrusheva TN. Extraction-pyrolytic method: fabrication of functional oxide materials (in Russian). Moskow: KomKniga. 2006.
[37] Serga V, Burve R, Maiorov M, Krumina A, Skaudžius R, Zarkov A, et al. Impact of gadolinium on the structure and magnetic properties of nanocrystalline powders of iron oxides produced by the extraction-pyrolytic method. Materials 2020;13:4147–57.
[38] Burve R, Serga V, Krumina A, Popļausks R. Preparation and characterization of nanocrystalline gadolinium oxide powders and films. Key Eng Mater 2020;850:267–72.
[39] Chornaja S, Sproge E, Dubencovs K, Kulikova L, Serga V, Cvetkovs A, et al. Selective oxidation of glycerol to glyceraldehyde over novel monometallic platinum catalysts. Key Eng Mater 2014;604:138–41.
[40] Serga V, Kulikova L, Cvetkov A, Krumina A. EPM fine-disperse platinum coating on powder carriers. IOP Conf Ser Mater Sci Eng 2012;38:012062.
[41] Serga V, Burve R, Krumina A, Romanova M, Kotomin EA, Popov AI. Extraction-pyrolytic method for TiO_2 polymorphs production. Crystals 2021;11(4):431–44.
[42] Gindin LM. Extraction processes and their applications (in Russian). Moskow: Nauka. 1984.
[43] Sharlo G. Methods of analytical chemistry. 1969. vol. 2 (in Russian). Moskow: Himija.
[44] Gribb AA, Banfield JF. Particle size effects on transformation kinetics and phase stability in nanocrystalline TiO_2. Am Mineral 1997;82(7–8):717–28.
[45] Rodionovs P, Jankovica D, Grabis J. Characteristics and photocatalytic activity of Sm doped ZnO nanoparticles. Key Eng Mater 2019;799:179–84.
[46] Akanni MS, Okoh EK, Burrows HD, Ellis HA. The thermal behaviour of divalent and higher valent metal soaps: review. Thermochim Acta 1992;208:1–40.

[47] Mehrotra RC, Bohra R. Metal carboxylates. London: Academic Press; 1983.
[48] Patil KC, Chandrashekhar GV, George MV, Rao CNR. Infrared spectra and thermal decompositions of metal acetates and dicarboxylates. Can J Chem 1968;46:257–65.
[49] Grivel JC. Thermal decomposition of $RE(C_2H_5CO_2)_3 \cdot H_2O$ (RE = Dy, Tb, Gd, Eu and Sm). J Therm Anal 2013;115(2):1253–64.
[50] Grivel JC, Zhao Y, Tang X, Pallewatta PGPA, Watenphul A. Thermal decomposition of heavy rare-earth butanoates, $Ln(C_3H_7CO_2)_3$ (Ln = Er, Tm, Yb and Lu) in argon. J Therm Anal 2016;126(3):1111–23.
[51] Štengl V, Bakardjieva S, Murafa N. Preparation and photocatalytic activity of rare earth doped TiO2 nanoparticles. Mater Chem Phys 2009;114(1):217–26.
[52] Mochizuki S, Suzuki Y, Nakanishi T, Ishi K. Valence-change and defect-induced white luminescence of Eu_2O_3. Phys B Condens Matter 2001;308–310:1046–9.
[53] Chattopadhyay AN, Dasgupta P, Jana YM, Ghosh D. A study on crystal field effect and single ion anisotropy in pyrochlore europium titanate (Eu2Ti2O7). J Alloys Compd 2004;384(1–2):6–11.
[54] Ghosh P, Patra A. Influence of surface coating on physical properties of TiO_2/Eu^{3+} nanocrystals. J Phys Chem C 2007;111(19):7004–10.
[55] Kawai T, Shimogaki A, Kifune K. Crystalline-phase dependent red luminescence of TiO_2:Eu^{3+} particles prepared by a sol–gel method. Phil Mag Lett 2008;88(1):1–7.
[56] Luo W, Li R, Liu G, Antonio MR, Chen X. Evidence of trivalent europium incorporated in anatase TiO2 nanocrystals with multiple sites. J Phys Chem C 2008;112(28):10370–7.
[57] Liu Y, Luo W, Zhu H, Chen X. Optical spectroscopy of lanthanides doped in wide band-gap semiconductor nanocrystals. J Lumin 2011;131(3):415–22.
[58] Li JG, Wang X, Watanabe K, Ishigaki T. Phase structure and luminescence properties of Eu^{3+}-doped TiO_2 nanocrystals synthesized by Ar/O_2 radio frequency thermal plasma oxidation of liquid precursor mists. J Phys Chem B 2006;110(3):1121–7.
[59] Frindell KL, Bartl MH, Robinson MR, Bazan GC, Popitsch A, Stucky GD. Visible and near-IR luminescence via energy transfer in rare earth doped mesoporous titania thin films with nanocrystalline walls. J Solid State Chem 2003;172(1):81–8. 2003.
[60] Xin H, Ma R, Wang L, Ebina Y, Takada K, Sasaki T. Photoluminescence properties of lamellar aggregates of titania nanosheets accommodating rare earth ions. Appl Phys Lett 2004;85(18):4187–9.